Published online 10 December 2015

Nucleic Acids Research, 2016, Vol. 44, No. 7 ***3045–3058***
doi: 10.1093/nar/gkv1350

Quantification of transcription factor-DNA binding affinity in a living cell

Sergey Belikov[1,*], Otto G. Berg[2] and Örjan Wrange[1,*]

[1]Department of Cell and Molecular Biology, Karolinska Institutet, SE-17177 Stockholm, Sweden and [2]Department of Cell and Molecular Biology, Uppsala University, BMC Box 596, SE-75124 Uppsala, Sweden

Received October 22, 2015; Revised November 18, 2015; Accepted November 19, 2015

ABSTRACT

The apparent dissociation constant (K_d) for specific binding of glucocorticoid receptor (GR) and androgen receptor (AR) to DNA was determined *in vivo* in *Xenopus* oocytes. The total nuclear receptor concentration was quantified as specifically retained [^{3}H]-hormone in manually isolated oocyte nuclei. DNA was introduced by nuclear microinjection of single stranded phagemid DNA, chromatin is then formed during second strand synthesis. The fraction of DNA sites occupied by the expressed receptor was determined by dimethylsulphate *in vivo* footprinting and used for calculation of the receptor-DNA binding affinity. The forkhead transcription factor FoxA1 enhanced the DNA binding by GR with an apparent K_d of ∼1 μM and dramatically stimulated DNA binding by AR with an apparent K_d of ∼0.13 μM at a composite androgen responsive DNA element containing one FoxA1 binding site and one palindromic hormone receptor binding site known to bind one receptor homodimer. FoxA1 exerted a weak constitutive- and strongly cooperative DNA binding together with AR but had a less prominent effect with GR, the difference reflecting the licensing function of FoxA1 at this androgen responsive DNA element.

INTRODUCTION

Gene regulation involves the sequence-specific DNA binding by proteins here dubbed transcription factors (TFs) in prokaryotic (1,2) and in eukaryotic cells (3,4). The modes of DNA binding of these TFs have been studied in detail *in vitro* (5,6) and by use of fluorescence techniques in live bacteria (7) and live eukaryotic cells (8). However, the estimation of the DNA binding affinity of a native TF to a defined DNA sequence *in vivo* in eukaryotes remains a challenge since it requires a quantitative analysis of (i) the intranuclear TF concentration, (ii) the concentration of specific DNA sites that are accessible for TF binding and (iii) the fraction of DNA sites bound by the TF. Furthermore, the eukaryotic genome is complex and each cell typically contains a large number of different DNA binding sites that are expected to have different affinities for a given TF. In metazoans the organization of the DNA in chromatin is exploited to gain tissue-specific gene regulation from a common genome (9) achieved by composite binding of different TFs to the regulatory DNA segments, i.e. enhancers (10). One class of TFs is dubbed pioneer TFs (11). They apparently have a stronger capacity to invade and bind their DNA targets in a chromatin context and to open the surrounding DNA segment for increased access of other TFs (12). FoxA1 is a well-known example of a pioneer factor (13) that plays a vital role in activation by several steroid receptors, including AR, ER and GR (14). Interestingly, a specific arrangement of FoxA1 and AR DNA binding sites was shown to be prevalent in prostate specific androgen responsive enhancers where FoxA1 qualified as a licensing factor (15).

The sequence specific DNA binding affinity between various TFs and their cognate DNA sites have been studied *in vitro* and their apparent K_d's were shown to be within or even below the nanomolar range (16–19). The analysis of TF-DNA binding *in vivo* have been performed based on fluorescence labeled TFs which allowed the estimation of the residence time from a cluster of binding sites (20). Such experiments demonstrated that the androgen receptor (AR) binds more strongly than GR to the hormone responsive enhancer of the mouse mammary tumor virus (MMTV) in mouse adenocarcinoma cells (21).

Based on our previous use of *Xenopus oocytes* in the analysis of TF-DNA binding and gene regulation (22,23) we decided to apply this system to address the DNA binding affinity for AR and GR *in vivo*. These gigantic oocytes allow protein(s) to be expressed at will by injection of corresponding *in vitro* transcribed mRNAs (24). The specific DNA binding sites are introduced by intranuclear injection of 1–10 ng of circular single-stranded (ss) DNA, which in our case yielded ∼0.3–3 × 10^9 gene copies. This injected DNA constitutes more than 99% of the total nuclear DNA since

*To whom correspondence should be addressed. Tel: +46 8 52487373; Fax: +46 8 339380; Email: orjan.wrange@ki.se
Correspondence may also be addressed to Sergey Belikov. Tel: +46 8 52487903; Fax: +46 8 339380; Email: sergey.belikov@ki.se
Present address: Sergey Belikov, Department of Molecular Biosciences, The Wenner-Gren Institute, Stockholm University, SE-106 91 Stockholm, Sweden.

© The Author(s) 2015. Published by Oxford University Press on behalf of Nucleic Acids Research.
This is an Open Access article distributed under the terms of the Creative Commons Attribution License (http://creativecommons.org/licenses/by-nc/4.0/), which permits non-commercial re-use, distribution, and reproduction in any medium, provided the original work is properly cited. For commercial re-use, please contact journals.permissions@oup.com

the oocyte nucleus contains only 37 pg of endogenous genomic DNA (25). Importantly, the introduction of ssDNA leads to second strand synthesis concomitantly with replication coupled chromatin assembly (26). The chromatin so obtained shares functional characteristics of that formed on stably transfected DNA in tissue culture cells (27). The DNA injected oocyte thus represents a live cell with a simple and well-defined DNA content containing the specific DNA binding site(s) at will. We used this system to analyze TF-DNA binding affinity of a prostate-specific androgen responsive DNA element (15). This has resulted in the first report on the affinity of a composite TF-DNA binding element *in vivo*. The difference observed between AR and GR affinity provides insight in the strong selective potential of a simple composite DNA element. This example offers a quantitative glimpse into the regulatory landscape of the eukaryotic genome where specific combinations of TFs are extracting the relevant genetic information for each cell type in metazoans (28).

MATERIALS AND METHODS

DNA constructs and nomenclature

The DNA reporter pMMTV:M13 contains the 1.2 kb of the MMTV long terminal repeat (MMTV LTR) fused to the Herpes Simplex virus Thymidine kinase (HSV TK) gene (29); its transfer to M13 was described (22). The MMTV enhancer mediates a hormone response by direct DNA binding of either AR (23) or GR (4) via a cluster of hexanucleotide repeats (TGTTCT-3′). This hexanucleotide binds one GR molecule thus constituting one binding element (BE). The *bona fide* DNA binding site of these steroid receptors harbors an imperfect palindrome consisting of two inverted BE-repeats arranged head to head with three intervening base pairs (bp) (Figure 2A). GR as well as AR binds cooperatively to such a DNA site as a homodimer (16,23). Here we refer to this binding site as a hormone response element (HRE). Its DNA sequence originates from an HRE located at −185/−171 relative to the transcription start site of the MMTV LTR (30), (c.f. Figure 2A). We inserted this HRE, dubbed HRE1/1 or a half HRE, HRE1/2, i.e. where the BE2 had been mutated in the pBlueScript^{TM} vector (see Figure 2A) in order to make ssDNA as phagemids (see below). These constructs also contained a FoxA1 consensus binding segment of 10 bp with four intervening bp on the 3′-side of the BE1 hexanucleotide (Figure 2A), an arrangement originating from genome wide analysis of AR and FoxA1 dependent gene regulation in murine prostate (15) and in human prostate cancer cells where FoxA1 acted as a licensing factor for AR-DNA binding (31). We included the FoxA1 site since many GR driven enhancers, including the MMTV enhancer, contains a cluster of FoxA1 sites (Holmqvist 2005) and FoxA1 stimulates GR- (24) as well as AR-mediated MMTV transcription (23). A search in the BlueScript vector DNA sequence using MatInspector version 9.3 (Genomatix, Germany) showed no significant binding sites for FoxA1 or AR/GR (data not shown).

pBS(GRE)7, a plasmid containing seven HREs, (Figure 1B) were ligated as direct repeats from annealed oligonucleotides flanked by asymmetric AvaI restriction sites as described (32) and then moved into pBlueScript between EcoR1 and HindIII restriction sites. Purified ssDNA from the filamentous phage M13 was purchased (USB, Affymetrix and New England Biolabs). Phagemid Bluescript ssDNA was propagated in E-coli DH5αF' using the helper phage VCSM13 (Agilent Technologies) and isolated as described (33) and the resulting ssDNA phagemid was checked by sequencing. These ssDNA preparations contained about 98% of the ssDNA phagemid and 2% of helper phage according to densitometry of agarose gels (not shown). See Supplementary Methods for further details as well as for mRNA production and *X. oocyte* preparations.

Quantification of intranuclear [GR] and [AR] in *Xenopus oocytes*

The AR and GR receptor proteins have one binding site for one molecule of steroid hormone. The hormone–receptor complex is translocated to the nucleus (34) where it is active in DNA binding (16,23). The synthetic glucocorticoid and androgen hormones Dexamethasone (Dex) and methyltrienolone (R1881), respectively, has a high affinity for their cognate ligand binding pocket and has a lower tendency for non-specific binding than naturally occurring hormone and these synthetic hormones were thus used in tritium-labeled form as probes to quantify the intranuclear amount of GR and AR protein, respectively. The large *X. oocyte* nuclei, ∼0.4 mm diameter, are isolated by manual dissection (35). See Supplementary Methods for further details and for estimation of intranuclear concentrations of expressed FoxA1.

Analysis of the intranuclear concentration of HRE

The DNA injected in single stranded form (ss) undergoes natural chromatin assembly that occurs during second strand synthesis, an efficient process that is completed within 4 h in *X. oocytes* (26). The dsDNA so obtained was extracted, purified and quantified using primer extension as described (34). Primer used: 'Reversed M13′: 5′AGCGGATAACAATTTCACACAGG-3′ (Supplementary Figure S1A). The nuclear DNA injection is done blindly and hence one can expect that not all ssDNA injections will end up in the nuclear compartment. To investigate how the injection of ssDNA in the cytosol would influence quantification of nuclear DNA we deliberately injected ssDNA into the cytosol and found that this DNA was not detectable after phenol extraction of whole oocytes the day after injection and hence it is apparently degraded. This infers that ssDNA that were injected into the cytosol instead of into the nucleus is lost and does not influence the analysis of the concentration of intranuclear dsDNA (data not shown). To compensate for variation in DNA content we routinely used 10–12 oocytes in each group and always analyzed double samples for both primer extension analysis of DNA amount and for dimethylsulphate (DMS) *in vivo* footprinting (see Figure 1 and Supplementary Figure S1). The variation of total DNA content originating from injected ssDNA when comparing the double samples was 8% or lower (data from Supplementary Figure S1). When analyzing 10 individual nuclei after injecting 4 ng of ssDNA we recovered dsDNA in all 10 nuclei but the DNA amount was variable, the result was 6.5 ng ±3.8 (average ± S.D., $n = 10$).

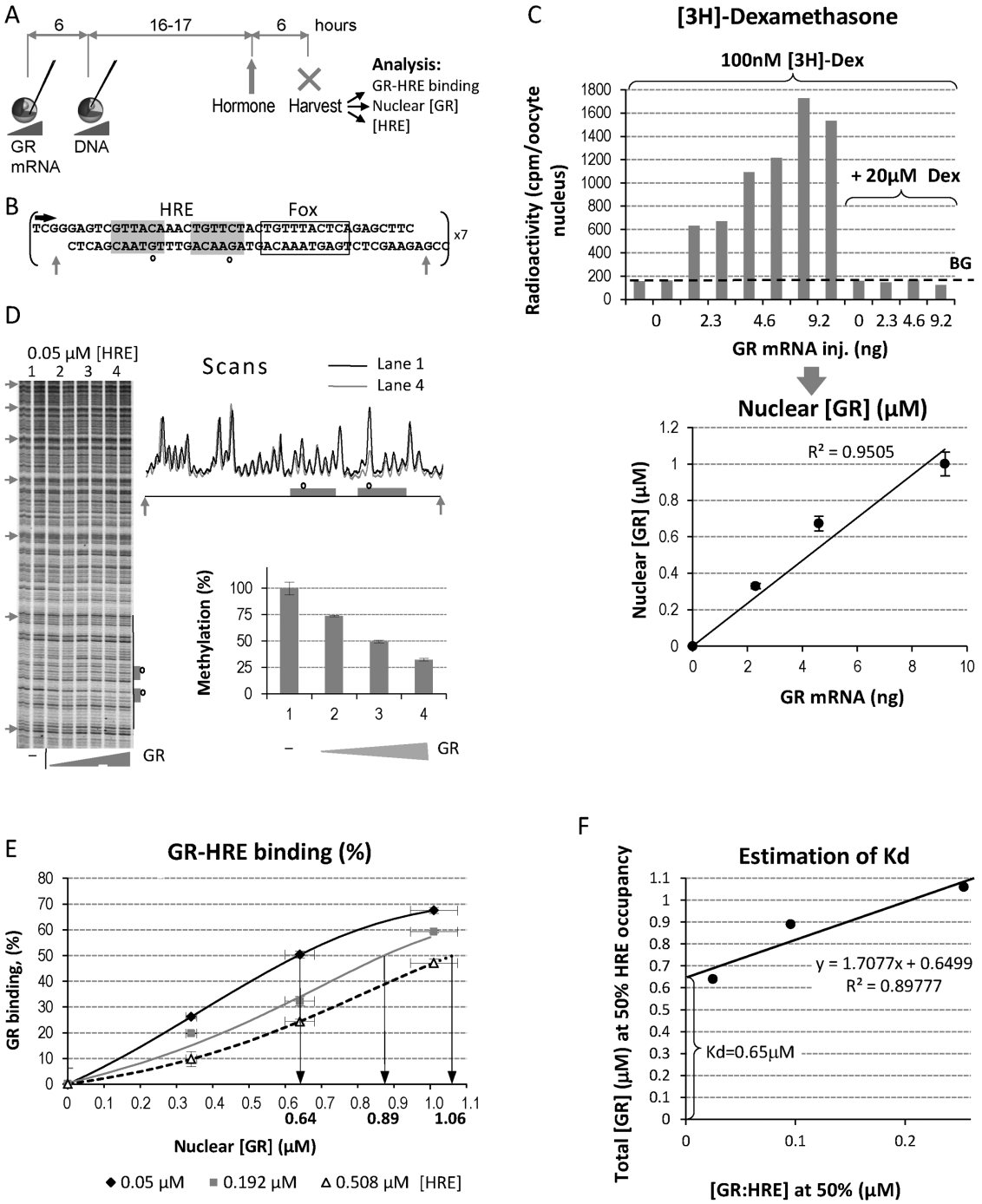

Figure 1. Apparent dissociation constant (K_d) analysis *in vivo* using three different concentrations of specific DNA sites in *Xenopus* oocytes. (**A**) Experimental design. (**B**) The pBS(HRE)x7 harbors seven repeats of the DNA segment, the partially palindromic HRE with its two binding elements (BE) highlighted in gray and a FoxA1 binding site is indicated by a rectangle. The protected guanines within the HRE are highlighted by empty circles and the direction of primer extension is shown by a black arrow. (**C**) Upper diagram, analysis of amount of [^{3}H]-Dex per oocyte nucleus in double samples after oocyte injection with indicated amount of GR mRNA (ng). Four samples were incubated with [^{3}H]-Dex supplemented with excess of unlabeled Dex. Stippled line indicates background that was subtracted. Lower diagram: nuclear GR concentration as a function of GR mRNA injection. (**D**) Autoradiogram showing the pattern of dimethylsulphate (DMS) methylation at increasing GR concentrations using 0.05 μM of HRE as shown in 1E, double samples for each GR concentration. Gray arrows show borders of the seven repeats, The HRE is indicated by two gray boxes with the protected bands as empty circles for the first repeat (to the right). Scans and columns illustrate quantification of methylation of corresponding guanines with error bars showing the average deviation of double samples. (**E**) GR-HRE binding analyzed by DMS methylation protection for three different concentrations of HRE as determined by primer extension (See also Supplementary Figure S1A). The concentration of nuclear GR required for 50% GR-HRE binding or DMS methylation protection, is highlighted by arrows pointing at the x-axis. The 50% binding of the 0.5 μM GRE curve was extrapolated from 47.2% binding at the highest GR concentration (dotted line). (**F**) Graphic estimation of K_d: when total nuclear GR concentration at 50% HRE binding is plotted as a function of the concentration of GR:HRE complex at 50% saturation then the free GR concentration present in absence of any GR:HRE complex is equal to the apparent K_d.

This demonstrates the level of reproducibility in achieving appropriately DNA injected nuclei.

DMS *invivo* footprinting

Analysis of the fraction of the specific DNA sites (HRE) that was bound by GR was done by the dimethylsulfate (DMS) *in vivo* footprinting technique as described before (34). See Supplementary Methods for further details.

Considerations of quantitative DMS *invivo* footprinting

The reduction in DMS mediated methylation of the two guanines contacted by the AR or GR on each DNA strand is assumed to directly reflect the level of DNA binding. However, a concern is that we rarely achieve 100% reduction of methylation even at concentrations were the increased receptor concentration reaches a plateau in terms of methylation protection. The usual level of maximal protection is about 40–70%, i.e. 30–60% DMS methylation still remains even at saturating levels of hormone receptor protein. In the experiments where titration of the receptor concentration reached a plateau of DNA binding we also calculated the apparent K_d based on the assumption that the level of DNA binding at the plateau represents 100% binding of the fraction of accessible DNA sites, (*F*acc) (see also 'Results' and 'Discussion' sections).

Experimental considerations

X enopus Laevis frogs are not genetically inbred and there is a 2–3-fold variation in the amount of protein expression when injecting the same mRNA into oocytes from different frogs (data not shown). Each oocyte is injected twice, first with mRNA and then with ssDNA (Figure 1A), the injections cause some trauma that adds to the variability. We handle this problem by injecting as many oocytes as possible for each experiment to include all controls and comparisons in one and the same preparation of oocytes and to have at least 10–12 oocytes in duplicates for each data point in the DMS *in vivo* footprinting assays. This has reduced the intra-experimental variability to acceptable levels as seen from double samples in our figures. However, some inter-experimental variation is seen and was controlled for by repeated experiments. Furthermore, the variable level of protein expression when using oocytes from different *Xenopus Laevis* frogs is a problem when injecting FoxA1 mRNA since too much FoxA1 expression may in fact inhibit GR-DNA interaction (36). This problem was dealt with by repeating the experiments where inappropriate high expression was achieved and hence an estimation of the levels of protein expression was important.

RESULTS

Analysis of the apparent K_d for GR-DNA binding *invivo*

GR was expressed by mRNA injection into the oocyte cytosol (Figure 1A) and quantified as specifically bound [^{3}H]-Dexamethasone ([^{3}H]-Dex) in nuclear extracts (Figure 1C). As a DNA binding target we constructed pBS(HRE)7, consisting of seven direct repeats of a partially palindromic hormone responsive element (from here on dubbed HRE) originating from the MMTV enhancer, which binds one GR-homodimer *in vitro* (16). This construct also contained a FoxA1 consensus binding site for future use (Figure 1B), however, later experiments showed no stimulation of GR binding by coexpression of FoxA1 with this pBS(HRE)7 construct (data not shown).

Three pools of *X. oocytes* were injected with increasing amounts of GR coding mRNA and then split in three subgroups and injected with increasing amounts of pBS(HRE)7 as ssDNA, 1, 4 or 10 ng, respectively. M13 ssDNA was added to the two lower concentrations of pBS(HRE)7 in order to keep the total amount of injected ssDNA constant (see Supplementary Figure S1A for details). DMS *in vivo* footprinting demonstrated distinct methylation protection of the expected guanines in the seven HRE repeats (Figure 1D, protected bands highlighted by empty circles). Both guanines, one in each of the two binding elements, (BEs defined in Figure 2A) were protected in parallel (Figure 1B and D and data not shown). The average pBS(HRE)7 DNA recovered from the oocytes rendered an intranuclear HRE concentration of 0.05, 0.19 and 0.50 μM, respectively (Supplementary Figure S1A). The nuclear GR-concentration dependent reduction in DMS methylation reflects specific GR-HRE binding (34) and hence the fraction of GR-bound HRE determined by DMS *in vivo* footprinting was plotted as a function of nuclear GR concentration (Figure 1E). As expected, a higher nuclear GR concentration was required to reach 50% saturation of the HRE sites when a higher concentration of HRE containing DNA was injected. The intranuclear GR concentrations required for 50% saturation of the specific DNA sites were estimated from the graphs as shown in Figure 1E, see vertical arrows.

The apparent K_d describing the specific binding affinity between GR and the HRE is defined as the nuclear concentration of GR not specifically bound to DNA that is required to reach 50% saturation of the HRE. Since the three intranuclear DNA concentrations are known (Supplementary Figure S1A), a diagram was designed presenting the total nuclear GR concentration required for 50% DNA binding as a function of the nuclear concentration of GR-HRE at 50% saturation (Figure 1F). In this diagram the three data points approaches a linear correlation that will intercept with the ordinate at the total nuclear GR concentration not specifically bound to the HRE, referred to as *Cf*, (Concentration free) that is required for 50% occupancy of the HRE and hence is equal to the apparent dissociation constant (K_d). The diagram shows that the apparent K_d is equal to 0.65 μM. The slope of the trendline is 1.7 indicating that there are about two GR entities that bind to each HRE as shown previously *in vitro* (16).

Using the Hill equation to analyze GR-HRE binding cooperativity and affinity

We rarely reach 100% methylation protection in our DMS *in vivo* footprinting experiments (see 'Materials and Methods' section and below). In several cases the DNA binding as a function of GR concentration reaches a plateau but

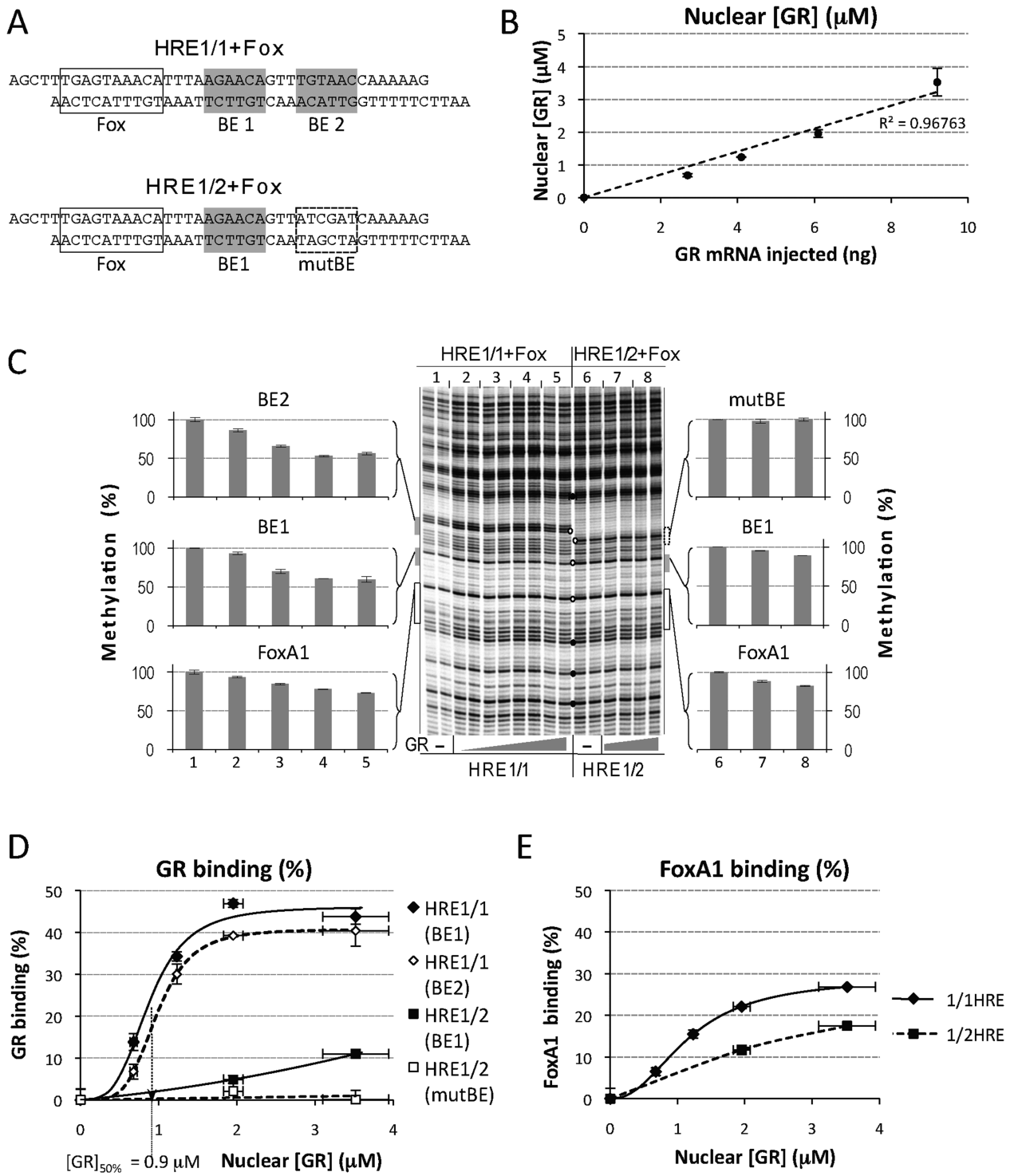

Figure 2. GR binding affinity to a complete HRE or a half HRE. (**A**) The DNA constructs used, the binding elements for GR and AR (BE1 and BE2) are highlighted in gray and the FoxA1 site indicated by a rectangle. These constructs are referred to in the text as HRE1/1 + Fox and HRE1/2 + Fox. (**B**) Nuclear GR concentration analyzed by [^{3}H]-Dex quantification in nuclear extracts. (**C**) Autoradiogram showing the pattern of DMS methylation, empty circles signify partially protected bands, unprotected bands used as reference are marked with black dots. Columns in the diagrams to the left and right illustrate quantification of DMS methylation with error bars showing the average deviation of double samples. (**D**) GR-HRE binding based on DMS methylation protection plotted as a function of nuclear GR concentration. (**E**) Binding activity at the FoxA1 site based on DMS methylation protection, presumably by a DNA binding protein of endogenous origin.

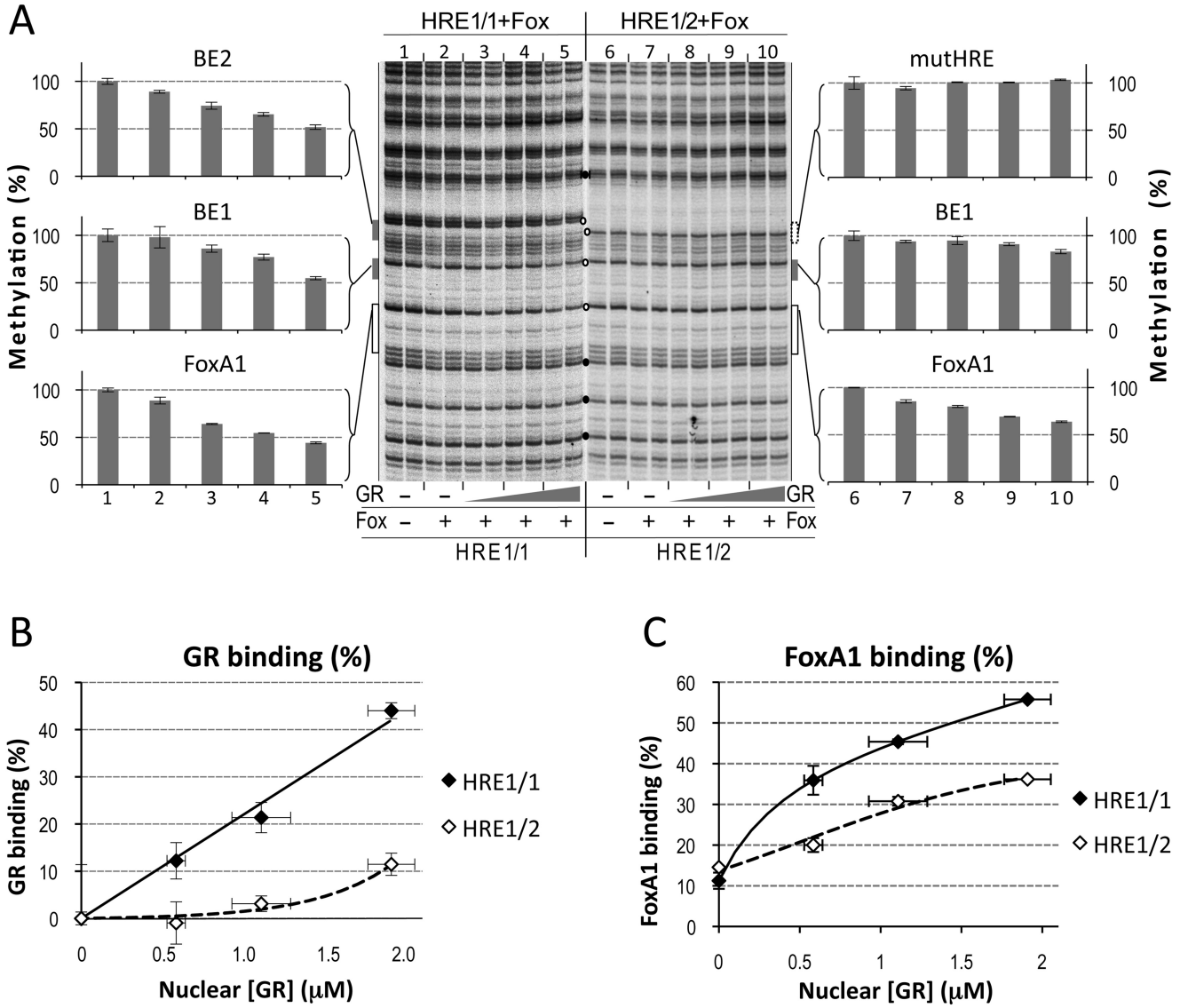

Figure 3. GR binding affinity to a complete HRE (HRE1/1 + Fox) and a half HRE (HRE1/2 + Fox) in presence of FoxA1 protein. Oocytes were injected with increasing amounts of GR mRNA, 3.5–8 ng, mixed with a constant amount of FoxA1 mRNA, 0.46 ng, resulting in 0.4 μM nuclear FoxA1 quantified as described (Supplementary Figure S3C). (**A**) Pattern of DMS methylation, as in Figure 2C. (**B**) GR-HRE binding based on DMS methylation protection of BE1 plotted as a function of nuclear GR concentration. (**C**) FoxA1-DNA binding based on DMS methylation protection plotted as a function of nuclear GR concentration.

the level of DMS methylation protection is still not 100% but more often lies within 40–80% (Figures 2D, 4C, 5B and D). In Figure 1E a 68% methylation protection is achieved, but this occur before the plateau is reached. These observations indicate that a fraction of the specific DNA sites may not be accessible for GR binding and thus should be ignored while calculating the affinity for the fraction of accessible sites (*F*acc). Thus we exploited the Hill equation in order to evaluate the level of cooperativity of GR-HRE interactions via analysis of the Hill coefficient (h) and to estimate the apparent K_d (Supplementary Figure S1B). By simulating the three different binding parameters, h, apparent K_d and *F*acc, we found that the best fit to the experimental data in Figure 1E was achieved with an estimated *F*acc close to 1.0, a Hill coefficient of 1.83 and an apparent K_d of 0.64 μM. As demonstrated in Supplementary Figure S1B, a nearly equally good fit is achieved when setting the *F*acc = 0.9, h = 2 and, thus, yielding the apparent $K_d = 0.57\mu M$.

An alternative strategy to calculate the apparent K_d

The apparent K_d for each data point in the diagram (Figure 1E) can be calculated based on the total nuclear GR concentration, the concentration of HRE sites and the fraction of the HRE sites occupied by GR, (Fb), as defined by DMS *in vivo* footprinting provided that the Hill coefficient is known (Supplementary Figure S1C). Calculation of the apparent K_d according to this formula for each data point in the diagram (Figure 1E) renders an average $K_d = 0.63 \pm 0.10$ μM

(mean ± S.D., $n = 9$) (Supplementary Figure S1C). An advantage with the use of the Hill plot for resolving the K_d is that it does not require previous knowledge about the level of cooperativity in the binding reaction and that a best fit simulation can be used to estimate the accessible HRE sites (*F*acc) as described in Supplementary Figure S1B.

This experiment also shows that a 10-fold increase in nonspecific M13-DNA injected and then recovered together with the specific pBS(HRE)7 DNA rendered virtually the same apparent *Kd* as in absence of M13-DNA (Supplementary Figure S1C).

Time of DMS methylation does not affect *F*acc

Why is the level of DMS methylation protection usually not involving more than 40–80% of the HRE (Figures 2D, 4C, 5B and D)? Could this be due to DMS methylation of the guanines within the HRE site is able to proceed during DMS exposure thus leading to a progressive block of the HRE sites? We addressed this question by analyzing the effect of increasing time of DMS exposure and found no time-dependent difference in the extent of GR-dependent methylation protection over the HRE (Supplementary Figure S1D). This result argues against significant impact of leaky DMS methylation during our experimental conditions.

GR binding to a complete HRE or a half HRE

The GR-DNA binding affinity was then addressed in a more defined context by construction of a complete and a half GR-DNA binding site also containing a FoxA1 site, here dubbed HRE1/1 + Fox and HRE1/2 + Fox, respectively, using the upstream strong HRE in the MMTV enhancer, as above, (Figure 2A and 'Materials and Methods' section). In the HRE1/2, the BE2 was mutated. The identical HRE1/2 sequence was previously shown to form a GR monomer complex *in vitro* (37). Both constructs contained a consensus FoxA1 site with a spacing of four base pairs between the BE1 and the FoxA1 site. This arrangement of an HRE and a FoxA1 site was previously reported to function in prostate specific AR response elements even when the FoxA1 site was adjacent to a half HRE (15).

DMS *in vivo* footprinting demonstrated a distinct GR binding at both BE1 and BE2 in a parallel fashion in the intact HRE1/1 + Fox but a very weak binding at the BE1 of the HRE1/2 + Fox (Figure 2C and D). GR binding to HRE1/1 + Fox plotted as a function of increasing nuclear GR concentration reached a plateau at ∼47% methylation protection (Figure 2D). This indicates that saturation of GR-HRE binding is achieved and argues for that about half of the HRE sites were not accessible for GR binding. We calculated the apparent K_d setting the 47% binding to 100% accessible sites (*F*acc = 0.47). This yielded an apparent K_d of 0.9 ± 0.15 μM (m ± S.D., $n = 3$) for the complete HRE1/1 + Fox palindrome assuming a 2-fold cooperativity ($h = 2$). This value is in good agreement with graphical estimation of the apparent K_d (Figure 2D, stippled line). For the HRE1/2 + Fox with a non-cooperative binding reaction ($h = 1$, see Supplementary Figure S1C), only a crude estimate is possible since there is no obvious plateau; assuming *F*acc = 1.0 we find a K_d of 17 ± 2 μM (mean ± average deviation, $n = 2$).

It was unexpected to see protection over the FoxA1 binding site since this protein was not expressed (Figure 2E). We assume that (an) endogenous protein(s), most probably member(s) of the forkhead protein family, may exert this effect. This unknown binding activity was clearly GR dependent since it increased with increasing GR binding to HRE1/1 as well as the HRE1/2 site.

GR-HRE binding in the presence of FoxA1

In an effort to monitor the GR-DNA binding affinity in the presence of FoxA1 we injected increasing amounts of GR mRNA together with a constant level of mRNA coding for FoxA1 (Figure 3A). Based on previous experiments where a higher nuclear concentration of FoxA1 caused inhibition on transcription (36), we aimed for a nuclear FoxA1 concentration near or below 1 μM monitored as described in Supplementary Methods. As illustrated by Figure 3C FoxA1 exerts a significant level of constitutive DNA binding in the absence of GR and its DNA binding is then increased in a GR-dependent fashion. The DMS *in vivo* footprinting analysis also revealed a distinct GR-HRE binding to the HRE + Fox. A more extensive analysis of this binding reaction is shown below (Figure 4C). We observed a much weaker binding of GR to the HRE1/2 + Fox containing a single BE1 (Figure 3A and B) that was previously shown to bind one GR monomer *in vitro* (37) and hence the formula for a non-cooperative binding was used and gave an apparent K_d = 25 ± 9 μM (mean ± average deviation, $n = 2$, assuming *F*acc = 1). However, this is only a crude estimation of the affinity since the actual *F*acc cannot be extracted from this dataset.

We conclude that the HRE1/2 + Fox is also able to bind GR albeit with a much reduced affinity than the intact HRE even in the presence of FoxA1 and that FoxA1 itself responds with an increased binding for its DNA site in the presence of GR thus suggesting a DNA binding cooperativity between FoxA1 and GR as shown previously to be the case for the MMTV promoter (24,38).

GR-DNA binding affinity to a complete HRE without any FoxA1 site

As demonstrated above (Figure 2C and E) we observed GR-dependent protection over the FoxA1 DNA binding site even in the absence of exogenously expressed FoxA1 thus implying an endogenous DNA binding activity. Indeed a database describing a list of proteins detected by mass spectrometry in *Xenopus* egg extracts contained several members of the forkhead box TF family (39). However, in our experience very little exogenously expressed FoxA1 causes a distinct increase in DNA binding at the FoxA1 site in the MMTV promoter and more importantly, FoxA1 expression has a robust stimulatory effect on glucocorticoid hormone driven transcription as well as GR-DNA binding (24,36). This argues that any endogenous DNA binding activity that interact with the FoxA1 DNA site does not share significant activity with FoxA1 in terms of stimulation of transcription. However, we cannot exclude that the observed endogenous

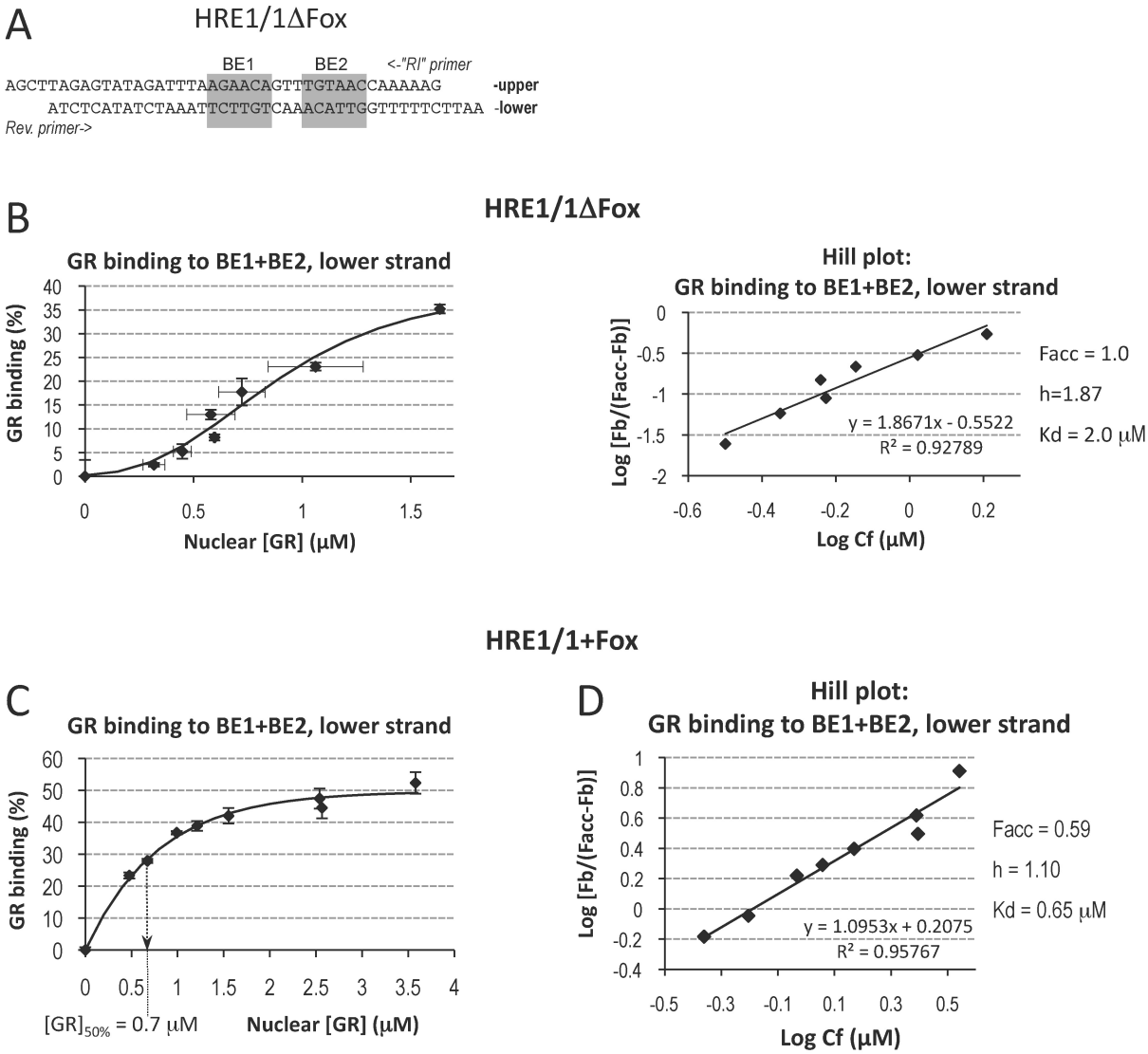

Figure 4. Comparison of GR-HRE binding without or with FoxA1. (**A**) The DNA construct HRE1/1ΔFox with a triple-point mutated FoxA1 site. (**B**) Oocytes injected with GR mRNA, 1.4–7 ng mRNA, followed by injection of ssHRE1/1ΔFox, 4 ng, were analyzed as in Figure 1A, the diagram shows the GR-DNA binding monitored by DMS methylation protection of corresponding guanines in BE1 and BE2 at lower strand as a function of nuclear GR concentration. A Hill plot is for the same data is shown to the right. (**C**) Oocytes injected with increasing GR mRNA, 1.5–9.2 ng and constant FoxA1 mRNA, 0.35 ng, followed by 4 ng ssDNA HRE1/1 + Fox injection and analyzed as in 4B. The oocytes contained 0.12 μM nuclear FoxA1 based on [^{14}C]-lysine labeled oocytes analyzed as described in Supplementary Figure S3C. (**D**) A Hill plot based on data in Figure 4C after introducing *F*acc = 0.59 in order to determine the K_d for the accessible HRE sites.

DNA binding activity at the FoxA1 site may exert an effect on the GR-DNA binding affinity in our experimental set up, especially so since this binding activity is increased with increased GR concentration (Figure 2E). In order to address the GR-HRE binding affinity in the absence of any adjacent TF-binding activity we constructed an HRE where the FoxA1 site was mutated, here called the HRE1/1ΔFox (Figure 4A).

Oocytes injected with increasing levels of GR mRNA showed a gradually increasing DMS methylation protection at the HRE (Figure 4B). Here we developed the methylation pattern with primers specific for both the upper strand (Supplementary Figure S2A) and the lower strand (Figure 4B). Both binding curves built on these data have a sigmoidal shape and Hill-plots rendered the same Hill coefficient of 1.87 arguing for a cooperative DNA binding as seen also in Figure 1 (Supplementary Figure S1B). The apparent K_d was calculated from the Hill plots and was in the range of 1.7–1.9 μM assuming that *F*acc = 1 (Supplementary Figure S2A). Since we did not reach saturation of the HRE site we addressed the minimal experimental *F*acc by setting the Hill coefficient to 2.0, which is the theoretically highest possible value for this system. This rendered a *F*acc = 0.77 and an apparent K_d of 1.6 μM (data not shown). We conclude that the apparent K_d for GR affinity to the naive HRE element is within the range of 1.6–1.9 μM and that the GR entities bind cooperatively to this site. An interesting observation from the GR-HRE1/1ΔFox binding curves in this experi-

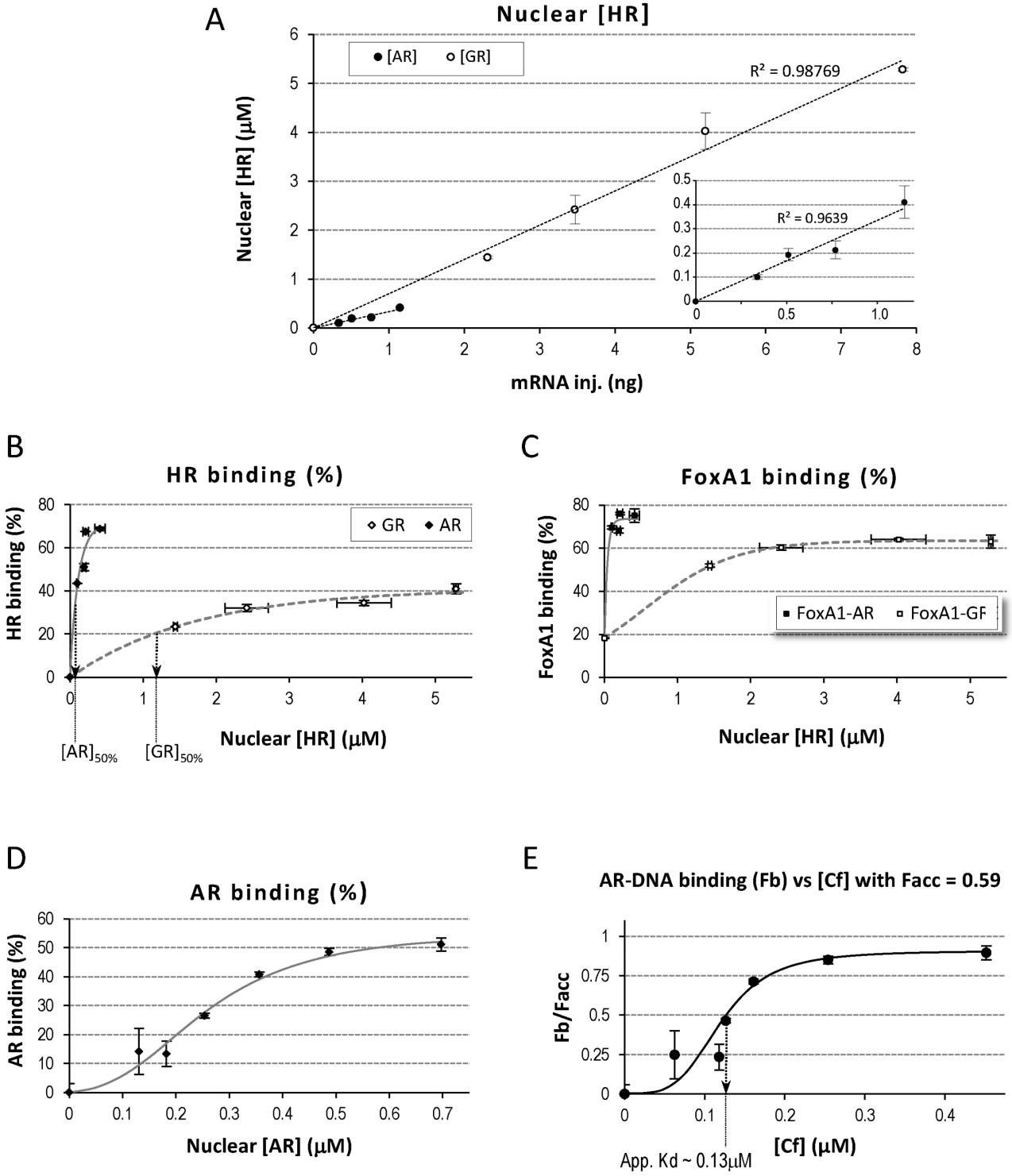

Figure 5. Comparison of AR- and GR-HRE binding to the HRE1/1 + Fox and in presence of FoxA1. (**A**) *Xenopus* oocytes were injected with 0.46 ng FoxA1 mRNA mixed with increasing amount of mRNA coding for either AR, 0.3–1.2 ng, or GR, 2.3–7.8 ng, followed by 4 ng of HRE1/1 + Fox ssDNA injection (Figure 2A). The intranuclear AR and GR concentration plotted as a function of injected mRNA, the inset diagram shows an expanded version of the AR diagram. Error bars signify average deviation of double samples. (**B**) HR-HRE binding based on DMS methylation protection at the HRE1/1 + Fox and plotted as a function of nuclear concentration of indicated HRs. The arrows show the graphically determined apparent K_d, i.e. the receptor concentration at 50% saturation of the HRE site. The nuclear HRE concentration was 0.12 μM (analyzed as in Supplementary Figure S1A). (**C**) FoxA1-DNA binding from the same experiment as shown in Figure 5A and B. (**D**) AR-DNA binding as a function of total nuclear AR concentration is shown, 0.2–0.69 μM of nuclear AR was expressed together with ∼0.6 μM FoxA1 and then 10 ng of ssDNA containing HRE1/1 + Fox was injected resulting in 0.24 μM of nuclear HRE. (**E**) Experiment described in Figure 5D. AR-HRE1/1 + Fox binding depicted as Fb/*F*acc plotted as function of Cf (i.e. nuclear AR not specifically bound to DNA). The stippled arrow indicates the graphically determined Cf at 50% GR-HRE binding, i.e the apparent K_d.

ment was that the methylation protection over the guanine in BE2 appeared to be delayed as compared to BE1 (Supplementary Figure S2D for details).

GR-HRE binding in presence of FoxA1

We repeated the GR titration with of HRE1/1 + Fox as previously described in Figure 3 but now with more data points in order to improve the analysis. As previously, the oocytes were injected with a constant concentration of FoxA1 mRNA together with increasing levels of GR mRNA. The binding curve shown in Figure 4C differs from that in the absence of FoxA1 by its hyperbolic, as oppose to sigmoidal, shape and also by approaching a plateau already at a GR concentration of 1.5–2 μM. Based on a best-fit analysis (see Supplementary Figure S1B) the saturation was estimated to occur at 59% DMS protection. This renders a Facc = 0.59 to be used for calculating the affinity for the accessible HRE sites. A Hill plot based on these terms results in a Hill coefficient of 1.1 and an apparent K_d of 0.65 μM (Figure 4D). The apparent K_d is in agreement with the graphical K_d extracted from the saturation curve at 50% binding (see vertical stippled grey arrow in Figure 4C and Supplementary Figure S2B). Since the fraction of GR bound to HRE was 3–9% of the total nuclear GR (data not shown) the values on the X-axis, i.e. free GR, are closely reflecting the Cf (Figure 4C). As described above (Figure 2D) there was no difference in the level of DNA binding when comparing DMS methylation protection in BE1 and BE2 (data not shown). Furthermore, FoxA1-DNA binding tracked the GR binding as seen in Figure 3 (compare Figure 4C to Supplementary Figure S2C).

The Hill plots, the binding curves and the apparent K_d values argues for that GR binding to the HRE differs depending on whether an assisting DNA binding activity such as FoxA1 is present (Figure 4C), or not (Figure 4B). However, the lack of GR:GR-cooperativity when binding to the HRE in the presence of FoxA1 (Figure 4C), based both on the Hill plot and the loss of a sigmoidal shape of the curve is a paradox, especially so since we see a parallel binding to the BE1 and BE2 while this is not the case in absence of FoxA1 where BE1 is occupied slightly before BE2 (Supplementary Figure S2D). We assume that the increased GR-HRE affinity in the presence of FoxA1 is caused by a FoxA1-dependent reduction of the chromatin-restricted DNA access, an effect caused by the constitutive FoxA1 binding to its DNA site close to the HRE. The mechanism behind the observed loss in GR-HRE cooperativity remains to be clarified.

AR binds the HRE with a much higher affinity than GR in presence of FoxA1

Since AR binds to the same DNA site as GR in the MMTV enhancer (23) and since AR was shown to have a slower dissociation rate than GR from the MMTV enhancer *in vivo* (21) we decided to compare the DNA binding affinity of AR and GR in parallel to the single HRE1/1 + Fox (shown in Figure 2A). Importantly, the HRE1/1 with a four bp spacing of the HRE from a FoxA1 site was adopted from a reported prostate-specific androgen response element (15,31).

Initial experiments where AR was expressed with FoxA1 showed that a drastic reduction of the amounts of AR was required to achieve intranuclear AR concentrations below the levels required for saturation of the HRE1/1 + Fox (Figure 5A and B). Here we compared AR-HRE and GR-HRE binding by injection of either mRNA to render 0.1–0.4 μM AR or 1.4–5.3 μM GR, respectively, based on the analysis of specific binding of [^{3}H]-R1881 or [^{3}H]-Dex, respectively, in manually isolated nuclei (Figure 5A). DMS methylation protection of oocytes expressing either AR or GR together with FoxA1 resulted in two very different dose-response curves, in each case with a plateau indicating saturation of the HRE-sites (Figure 5B). That the apparent DNA binding affinity is much stronger for AR as compared to GR is obvious from the binding curves (Figure 5B). We also note a receptor-specific difference for the Facc since ∼70% of the HRE sites are saturated in the AR experiment while 40% of the HRE sites are saturated by GR.

The nuclear FoxA1 concentration was 1.1 μM when analyzed by densitometry of [^{14}C]-lysine labeled oocytes as described (Supplementary Methods). The DNA binding of FoxA1 revealed the same difference in affinity when comparing its binding in either AR or GR context (Figure 5C) as the receptor-DNA binding curves with the only difference being that FoxA1 also had a constitutive DNA binding activity which was in agreement with previous results (c.f. Figure 3C and Supplementary Figure S2C). The binding curves reached a plateau in both cases and we graphically estimated total nuclear receptor concentration at 50% binding for GR to ∼1.2 μM, the corresponding value for AR-HRE binding appeared to be about an order of magnitude lower (Figure 5B, stippled arrows defining the value on abscissa for 50% binding). We note that more than 50% of the total nuclear AR is specifically bound to the HRE1/1 before the plateau is reached in the binding curve. In case of GR about 4% of the GR molecules are specifically bound at the lowest GR concentration (data not shown). This large difference in the fraction of HRE bound receptor is a consequence of the much higher affinity of the AR–DNA interaction in this particular FoxA1 context.

The intranuclear AR quantification data had lower accuracy than for GR since the lowest AR concentration contained only about a 2-fold higher amount of radioactive hormone as compared to the background radioactivity in non-injected oocyte nuclei (Figure 5A, and data not shown). For this reason the experiment was repeated using 10 ng of injected ssDNA harboring the HRE1/1 + Fox as DNA target. The higher HRE concentration would require a higher AR and hence the accuracy of the intracellular AR concentration might be improved (Supplementary Figure S3A and B). The binding curve so obtained was plotted as a function of total nuclear AR concentration (Figure 5D). After subtraction of the HRE-bound AR a DNA-binding curve was plotted as a function of the free nuclear AR concentration (Cf) (Figure 5E) and rendered an apparent K_d of ∼0.13 μM when estimated graphically from the non-bound AR (Cf) at 50% saturation of the DNA sites. A best fit analysis of the data in Figure 5E (Supplementary Figure S1B) assuming $h = 2$, yielded similar result, i.e. K_d = 0.14 μM and Facc = 0.59 and $h = 2$ (not shown).

We also addressed the AR-DNA binding affinity to the half site HRE1/2 + Fox. This experiment was done at saturating AR concentrations of 0.48 and 1.4 μM nuclear AR in presence or absence of FoxA1 (Figure 6A) making the calculation of the apparent K_d unreliable. However, this experiment revealed a 3.5-fold FoxA1-dependent stimulation of AR-DNA binding to HRE1/1 + Fox while the AR binding to HRE1/2 + Fox was completely dependent on FoxA1 and reached less than half of the HRE binding seen for the complete HRE. Interestingly, the composite AR and FoxA1 binding to HRE1/2 + Fox seem to be more robust than the binding of GR and FoxA1 to this target (Figure 3B). In this context we reconcile that the HRE1/2 + Fox is a prevalent androgen-responsive elements in the prostate in combination with a FoxA1 positioned in the same place relative to the HRE1/2 as used here (15). The FoxA1 binding follows the AR binding curves for HRE1/1 and HRE1/2 if correcting for the level of constitutive DNA binding (Figure 6B). As reported above (Figure 2E) there was an endogenous DNA binding activity seen at the FoxA1 site when FoxA1 was not expressed, this activity also followed the level of AR binding (Figure 6B).

The effects of FoxA1 on AR-DNA binding was also addressed by expressing increasing concentrations of AR in the presence of 0; 0.55 or 1.1 μM FoxA1 and then monitoring DNA binding to the HRE1/1 + Fox. As shown in Supplementary Figure S3C the AR-HRE binding in absence of FoxA1 was barely detectable at these lower AR concentrations but was robustly stimulated by the presence of 0.55 μM FoxA1. However, this level of AR-DNA binding was reduced at the highest AR concentration (Supplementary Figure S3C, stippled line). When the intranuclear FoxA1 concentration was increased to 1.1 μM then the AR-DNA binding increased further at the highest AR concentration with a tendency to approach a plateau. This experiment was reproduced with similar result (not shown). Collectively this shows that FoxA1 is strongly enhancing the AR-DNA binding activity at the HRE1/1 + Fox site. Importantly, there was no stimulation of AR-DNA binding by the presence of FoxA1 when the HREΔFox DNA was used (data not shown).

We conclude that AR binds to the HRE1/1 + Fox (Figure 2A) with an order of magnitude higher apparent affinity than GR (Figure 5B) albeit this requires the presence of FoxA1 and its DNA binding site adjacent to the receptor binding DNA site to form a composite AR response element. These results are in agreement with the reported FoxA1 licensing activity for AR binding to tissue specific androgen-hormone responsive enhancers in the murine prostate (15) and in prostate cancer cells (31).

DISCUSSION

Is it relevant to use *X. oocytes* to study the effect of chromatin on DNA binding? The chromatin structure in a differentiated metazoan cell contains many specialized domains characterized by different levels of DNA accessibility (40). Single stranded DNA injection into the nucleus of *X. oocytes* results in formation of homogeneous chromatin after second strand synthesis as demonstrated by digestion with MNase (24) and DNaseI as well as other studies of GR-mediated chromatin remodeling and transcription (22). Oocytes lack somatic linker histones but contain an oocyte specific linker histone, B4; however, if a somatic linker histone H1 is introduced into *X. oocytes* it causes a slightly enhanced GR binding to the MMTV enhancer (41).

Importantly, there is a time dependent decrease in DNA access in chromatin formed by injected ssDNA in *X. oocytes* after second strand synthesis due to a progressive histone deacetylation. This process correlates with a reduced GR-DNA binding and a reduced level of hormone activation from the MMTV promoter (35). It dictates keeping the time after DNA injection constant, here we allowed 22–23 h from ssDNA injection to harvest (Figure 1A). However, we observed an inter-experimental variation in the fraction of accessible HREs (*F*acc) probably implicating variability in the deacetylation rate thus resulting in a variation in TF-DNA access (22,35). Taken together we assume that the chromatin structure in *X. oocytes* may serve as a model for an open or active chromatin domain, as oppose to densely packed and silent chromatin.

An important advantage with *X. oocytes* is that the intranuclear TF amount may be quantified after manual isolation of the oocyte nucleus (Figure 1C). In addition, the intranuclear DNA injection allows the formation of a live cell with a genome of unparalleled simplicity; this allows specific DNA binding to be quantified by DMS *in vivo* footprinting. Previous reports have demonstrated that mammalian cells may contain up to $\sim 10^5$ of GR molecules or other steroid receptors per cell (42). Hormone-dependent translocation of these receptors into the cell nucleus with a diameter of 6 μm renders an intranuclear concentration of ~1.5 μM. The DNA concentration of a human cell with a diploid genome of 6.4×10^9 bp and a nuclear diameter of 6 μm contains 94 mM DNA, (bp). The endogenous 37 pg of DNA in a *X. oocyte* (25) renders a DNA concentration of 1.4 μM and injection of ss plasmid to obtain 5 ng of ds-DNA results in 0.2 mM DNA (bp). We conclude that the TF concentrations used in our experiments are within the range of a mammalian cell while the total DNA concentration in oocyte nuclei is considerably lower.

The DMS-dependent methylation of DNA is initiated in the live cell 6 h after addition of hormone when equilibrium between DNA and the TF(s) is already established; this equilibrium was not affected by the time of DMS incubation (Supplementary Figure S1D). Notably, the level of methylation protection at saturation was different in the same pool of oocytes when comparing AR and GR binding in presence of FoxA1 where saturation was achieved at 70 and 40%, respectively (Figure 5B and 'Results' section). Furthermore, different concentrations of FoxA1 in combination with different receptors or different HREs resulted in different degree of access to the nuclear HRE sites (Figure 6 and Supplementary Figure S3C). We also observed, that the fraction of accessible HRE sites for a specific combination of receptor and FoxA1 was different in different oocyte preparations (See 'Materials and Methods' section on inter-experimental variation in *X. oocytes*). This indicates that other endogenous factors, such as various co-activators and/or chromatin remodeling complexes, recruited by either AR or GR with or without an adjacently DNA-bound FoxA1, may influence the DNA bind-

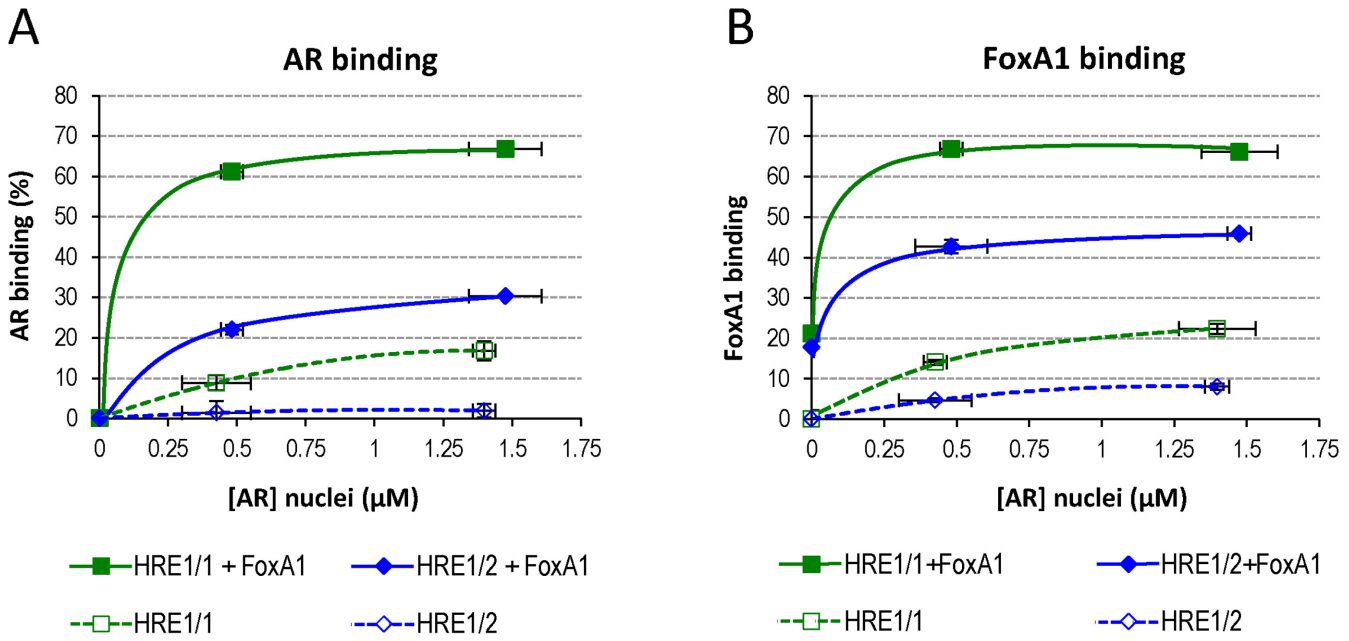

Figure 6. FoxA1 drastically enhances AR binding to HRE1/1 + Fox and HRE1/2 + Fox constructs. Groups of oocytes were mRNA injected to express AR or AR together with FoxA1 followed by nuclear injection of HRE1/1 + Fox or HRE1/2 + Fox constructs. (**A**) AR-HRE binding based on DMS methylation protection plotted as a function of nuclear AR concentration. (**B**) FoxA1-DNA binding based on DMS methylation protection plotted as a function of nuclear AR concentration.

ing event. We propose that when calculating the apparent K_d, the fraction of accessible HRE defined by an approaching plateau, i.e. saturation of accessible HRE sites, should be regarded as the total available HRE. With this view the variation in the level of plateau formation can be corrected for as described in Supplementray Figure S1B (See also Figures 2D, 4C and 5E), while this becomes difficult when a plateau is not reached (Figure 3B). The HRE sites that are not accessible in a given TF-DNA binding context describe the equilibrium between the chromatin insulating capacity and the counteracting DNA binding activity. We show here that a change either in the TF context or the DNA target will alter this equilibrium, and hence the DNA accessibility and the level of the plateau formation (Figures 5B, 6A and Supplementary Figure S3C). Positioning of nucleosomes is unlikely to modulate the level of accessibility since we showed that they are randomly positioned on injected DNA before hormone induction and that positioning is induced by the TF-DNA binding (22,24).

The fact that AR-DNA binding in the presence of FoxA1 was an order of magnitude stronger than the GR-DNA binding at the composite HRE1/1 + Fox highlights the selective power of protein–DNA interaction in chromatin (Figure 5B and E). Importantly, the composite HRE used here, also containing a FoxA1 DNA binding site (Figure 2A), mimicked a previously described androgen responsive element that was revealed by a genome wide mapping of prostate-specific AR binding elements where FoxA1 was required as a licensing factor (15,31). Apparently, the spatial arrangement of the two binding sites for AR and FoxA1 was suitable for strong cooperative binding. As defined by the apparent K_d we show that half of the specific HRE sites will be occupied at 0.13 μM concentration of free nuclear AR. We speculate that the concentration range of AR used here may approach the physiological concentration range to be required for productive binding *in vivo*. This does not exclude that composite binding sites in active enhancers may have higher affinities than demonstrated here. Conversely, significant GR-DNA binding to the same site with the apparent K_d of ∼1 μM described in this work may be too low for a significant DNA binding to occur in the living cell. Previous work has shown that GR-binding enhancers contain strongly conserved composite GR-binding sites (10) and that half GR-binding sites regulate specific target genes (43). We assume that GR will bind to composite GR-responsive elements with a similar affinity as the AR and FoxA1 binding to HRE1/1 + Fox shown here (Figure 5) if provided with the appropriate combination of TF binding-partner(s) to match the composite enhancer element.

Previous GR binding experiments using either naked (16,17), or *in vitro* reconstituted nucleosomal (44), MMTV enhancer DNA rendered an apparent K_d of 0.3 and 0.7 nM, respectively, which is about three orders of magnitude higher affinity than seen in our *in vivo* experiments concerning GR (see 'Results' section). This discrepancy illustrates the effect of chromatin in combination with the intranuclear physicochemical conditions of a live cell, conditions that will be difficult to reconstruct *in vitro.* For example, polyamines are present in high concentrations in all cells (45) and were shown to modulate histone–DNA interactions and to act as repressors for certain protein–DNA interactions *in vivo* (46). We speculate that the intranuclear environment and the histone–DNA interactions set the threshold for the DNA access thereby promoting selectivity in the TF–DNA interactions. The comparison of

AR and GR DNA binding in presence of FoxA1 (Figure 5B) illustrates the selective power of a composite HRE to mediate an AR- rather than a GR response, but also the possibility for a high enough concentrations of GR to bind this AR-responsive site as was shown to sometimes occur in prostate cancer cells (47). A strict control of the intracellular concentration of TFs for each cell type thus becomes an important factor for maintaining a stable differentiation (28).

The pioneer factors, such as FoxA1, preset the chromatin structure (11), facilitate binding of other TFs such as steroid receptors and may serve as a licensing factor in a particular context (14,15). Our results are compatible with such a mechanism since we see a distinct constitutive FoxA1 binding capacity (c.f. Figures 3C, Figure 5C and Supplementary Figures S3B and S4D) as well as a strong cooperative binding component of FoxA1 which tracks the binding of the adjacent receptor as seen from comparison of FoxA1 binding together with either AR or GR (Figure 5B and C). It may be a common feature in cellular differentiation that a pioneer factor specifies a celltype-specific pattern of partly open chromatin domains. An example of this is the TF called Meis that seem to act as a pioneer factor by mediating a presetting state of certain enhancers defining body segments during vertebrate development and where a subset of these sites that contain the proper Hox motifs are bound by the homeobox factor Hoxa2 that selectively enhances genes defining the body segment of the second branchial arch (48).

By adopting the *X. oocytes in vivo* system we can for the first time report the sequence-specific TF-DNA binding affinity, specifically the apparent K_d, in a living cell. Furthermore, we demonstrated a strong selectivity for AR over GR binding to a previously described androgen response element involved in prostate-specific gene expression *in vivo* (15). This selectivity relies on the arrangement of the pioneer factor FoxA1 binding site in relation to the HRE since the receptor binding DNA segment as such is not different for AR and GR (31). The quantification of the DNA binding affinities for different TFs at their enhancer-binding DNA sites *in vivo* will increase the understanding of the target selection mechanisms in eukaryotic genomes.

SUPPLEMENTARY DATA

Supplementary Data are available at NAR Online.

ACKNOWLEDGEMENTS

Ö.W. wants to thank Dr Maria Falkenberg and Dr Javier Miralles Fusté, Department of Biochemistry and Cell Biology University of Gothenburg, for help and advice to prepare phagemids and to purify ssDNA. Dr Björn Reinius is gratefully acknowledged for advice and analysis of TF binding sites using the Matinspector software. As an associate member ÖW acknowledges the European Commission Network of Excellence, EpiGeneSys.

FUNDING

Swedish Cancer Society [14 0792 to S.B., Ö.W.]. Funding for open access charge: Swedish Cancer Society [140792].

Conflict of interest statement. None declared.

REFERENCES

1. Ptashne,M. (1967) Specific binding of the lambda phage repressor to lambda DNA. *Nature*, **214**, 232–234.
2. Ogata,R.T. and Gilbert,W. (1978) An amino-terminal fragment of lac repressor binds specifically to lac operator. *Proc. Natl. Acad. Sci. U.S.A.*, **75**, 5851–5854.
3. Myers,R.M., Rio,D.C., Robbins,A.K. and Tjian,R. (1981) SV40 gene expression is modulated by the cooperative binding of T antigen to DNA. *Cell*, **25**, 373–384.
4. Payvar,F., Wrange,O., Carlstedt-Duke,J., Okret,S., Gustafsson,J.A. and Yamamoto,K.R. (1981) Purified glucocorticoid receptors bind selectively in vitro to a cloned DNA fragment whose transcription is regulated by glucocorticoids in vivo. *Proc. Natl. Acad. Sci. U.S.A.*, **78**, 6628–6632.
5. Johnson,A.D., Poteete,A.R., Lauer,G., Sauer,R.T., Ackers,G.K. and Ptashne,M. (1981) lambda Repressor and cro–components of an efficient molecular switch. *Nature*, **294**, 217–223.
6. von Hippel,P.H. and Berg,O.G. (1986) On the specificity of DNA-protein interactions. *Proc. Natl. Acad. Sci. U.S.A.*, **83**, 1608–1612.
7. Hammar,P., Leroy,P., Mahmutovic,A., Marklund,E.G., Berg,O.G. and Elf,J. (2012) The lac repressor displays facilitated diffusion in living cells. *Science*, **336**, 1595–1598.
8. Chen,J., Zhang,Z., Li,L., Chen,B.C., Revyakin,A., Hajj,B., Legant,W., Dahan,M., Lionnet,T., Betzig,E. *et al.* (2014) Single-molecule dynamics of enhanceosome assembly in embryonic stem cells. *Cell*, **156**, 1274–1285.
9. John,S., Sabo,P.J., Johnson,T.A., Sung,M.H., Biddie,S.C., Lightman,S.L., Voss,T.C., Davis,S.R., Meltzer,P.S., Stamatoyannopoulos,J.A. *et al.* (2008) Interaction of the glucocorticoid receptor with the chromatin landscape. *Mol. Cell*, **29**, 611–624.
10. So,A.Y., Chaivorapol,C., Bolton,E.C., Li,H. and Yamamoto,K.R. (2007) Determinants of cell- and gene-specific transcriptional regulation by the glucocorticoid receptor. *PLoS Genet.*, **3**, e94.
11. Iwafuchi-Doi,M. and Zaret,K.S. (2014) Pioneer transcription factors in cell reprogramming. *Genes Dev.*, **28**, 2679–2692.
12. Soufi,A., Garcia,M.F., Jaroszewicz,A., Osman,N., Pellegrini,M. and Zaret,K.S. (2015) Pioneer transcription factors target partial DNA motifs on nucleosomes to initiate reprogramming. *Cell*, **161**, 555–568.
13. McPherson,C.E., Shim,E.Y., Friedman,D.S. and Zaret,K.S. (1993) An active tissue-specific enhancer and bound transcription factors existing in a precisely positioned nucleosomal array. *Cell*, **75**, 387–398.
14. Pihlajamaa,P., Sahu,B. and Janne,O.A. (2015) Determinants of receptor- and tissue-specific actions in androgen signaling. *Endocr. Rev.*, **36**, 357–384.
15. Pihlajamaa,P., Sahu,B., Lyly,L., Aittomaki,V., Hautaniemi,S. and Janne,O.A. (2014) Tissue-specific pioneer factors associate with androgen receptor cistromes and transcription programs. *EMBO J.*, **33**, 312–326.
16. Wrange,O., Eriksson,P. and Perlmann,T. (1989) The purified activated glucocorticoid receptor is a homodimer. *J. Biol. Chem.*, **264**, 5253–5259.
17. Perlmann,T., Eriksson,P. and Wrange,O. (1990) Quantitative analysis of the glucocorticoid receptor-DNA interaction at the mouse mammary tumor virus glucocorticoid response element. *J. Biol. Chem.*, **265**, 17222–17229.
18. Fried,M.G. and Crothers,D.M. (1984) Equilibrium studies of the cyclic AMP receptor protein-DNA interaction. *J. Mol. Biol.*, **172**, 241–262.
19. Berg,O.G. and von Hippel,P.H. (1988) Selection of DNA binding sites by regulatory proteins. II. The binding specificity of cyclic AMP receptor protein to recognition sites. *J. Mol. Biol.*, **200**, 709–723.
20. McNally,J.G., Muller,W.G., Walker,D., Wolford,R. and Hager,G.L. (2000) The glucocorticoid receptor: rapid exchange with regulatory sites in living cells. *Science*, **287**, 1262–1265.
21. Nenseth,H.Z., Dezitter,X., Tesikova,M., Mueller,F., Klokk,T.I., Hager,G.L. and Saatcioglu,F. (2014) Distinctly different dynamics and kinetics of two steroid receptors at the same response elements in living cells. *PLoS One*, **9**, e105204.

22. Belikov,S., Gelius,B., Almouzni,G. and Wrange,O. (2000) Hormone activation induces nucleosome positioning in vivo. *EMBO J.*, **19**, 1023–1033.
23. Belikov,S., Oberg,C., Jaaskelainen,T., Rahkama,V., Palvimo,J.J. and Wrange,O. (2013) FoxA1 corrupts the antiandrogenic effect of bicalutamide but only weakly attenuates the effect of MDV3100 (Enzalutamide). *Mol. Cell Endocrinol.*, **365**, 95–107.
24. Belikov,S., Astrand,C. and Wrange,O. (2009) FoxA1 binding directs chromatin structure and the functional response of a glucocorticoid receptor-regulated promoter. *Mol. Cell. Biol.*, **29**, 5413–5425.
25. Hausen,P. and Riebesell,M. (1991) *The early developemnt of Xenopus Laevis, an atlas of the histology*. Springer-Verlag, Berlin Heidelberg; NY.
26. Almouzni,G. and Wolffe,A.P. (1993) Replication-coupled chromatin assembly is required for the repression of basal transcription in vivo. *Genes Dev.*, **7**, 2033–2047.
27. Li,J., Fu,J., Toumazou,C., Yoon,H.G. and Wong,J. (2006) A role of the amino-terminal (N) and carboxyl-terminal (C) interaction in binding of androgen receptor to chromatin. *Mol. Endocrinol.*, **20**, 776–785.
28. Holmberg,J. and Perlmann,T. (2012) Maintaining differentiated cellular identity. *Nat. Rev. Genet.*, **13**, 429–439.
29. Buetti,E. and Kuhnel,B. (1986) Distinct sequence elements involved in the glucocorticoid regulation of the mouse mammary tumor virus promoter identified by linker scanning mutagenesis. *J. Mol. Biol.*, **190**, 379–389.
30. Payvar,F., DeFranco,D., Firestone,G.L., Edgar,B., Wrange,O., Okret,S., Gustafsson,J.A. and Yamamoto,K.R. (1983) Sequence-specific binding of glucocorticoid receptor to MTV DNA at sites within and upstream of the transcribed region. *Cell*, **35**, 381–392.
31. Sahu,B., Laakso,M., Pihlajamaa,P., Ovaska,K., Sinielnikov,I., Hautaniemi,S. and Janne,O.A. (2013) FoxA1 specifies unique androgen and glucocorticoid receptor binding events in prostate cancer cells. *Cancer Res.*, **73**, 1570–1580.
32. Li,Q. and Wrange,O. (1993) Translational positioning of a nucleosomal glucocorticoid response element modulates glucocorticoid receptor affinity. *Genes Dev.*, **7**, 2471–2482.
33. Yamamoto,K.R., Alberts,B.M., Benzinger,R., Lawhorne,L. and Treiber,G. (1970) Rapid bacteriophage sedimentation in the presence of polyethylene glycol and its application to large-scale virus purification. *Virology*, **40**, 734–744.
34. Belikov,S., Gelius,B. and Wrange,O. (2001) Hormone-induced nucleosome positioning in the MMTV promoter is reversible. *EMBO J.*, **20**, 2802–2811.
35. Astrand,C., Belikov,S. and Wrange,O. (2009) Histone acetylation characterizes chromatin presetting by NF1 and Oct1 and enhances glucocorticoid receptor binding to the MMTV promoter. *Exp. Cell Res.*, **315**, 2604–2615.
36. Belikov,S., Holmqvist,P.H., Astrand,C. and Wrange,O. (2012) FoxA1 and glucocorticoid receptor crosstalk via histone H4K16 acetylation at a hormone regulated enhancer. *Exp. Cell Res.*, **318**, 61–74.
37. Eriksson,P. and Wrange,O. (1990) Protein-protein contacts in the glucocorticoid receptor homodimer influence its DNA binding properties. *J. Biol. Chem.*, **265**, 3535–3542.
38. Holmqvist,P.H., Belikov,S., Zaret,K.S. and Wrange,O. (2005) FoxA1 binding to the MMTV LTR modulates chromatin structure and transcription. *Exp. Cell Res.*, **304**, 593–603.
39. Wuhr,M., Freeman,R.M. Jr, Presler,M., Horb,M.E., Peshkin,L., Gygi,S.P. and Kirschner,M.W. (2014) Deep proteomics of the Xenopus laevis egg using an mRNA-derived reference database. *Curr. Biol.*, **24**, 1467–1475.
40. Filion,G.J., van Bemmel,J.G., Braunschweig,U., Talhout,W., Kind,J., Ward,L.D., Brugman,W., de Castro,I.J., Kerkhoven,R.M., Bussemaker,H.J. *et al.* (2010) Systematic protein location mapping reveals five principal chromatin types in Drosophila cells. *Cell*, **143**, 212–224.
41. Belikov,S., Astrand,C. and Wrange,O. (2007) Mechanism of histone H1-stimulated glucocorticoid receptor DNA binding in vivo. *Mol. Cell. Biol.*, **27**, 2398–2410.
42. Biggin,M.D. (2011) Animal transcription networks as highly connected, quantitative continua. *Dev. Cell*, **21**, 611–626.
43. Schiller,B.J., Chodankar,R., Watson,L.C., Stallcup,M.R. and Yamamoto,K.R. (2014) Glucocorticoid receptor binds half sites as a monomer and regulates specific target genes. *Genome Biol.*, **15**, 418–433.
44. Perlmann,T. (1992) Glucocorticoid receptor DNA-binding specificity is increased by the organization of DNA in nucleosomes. *Proc. Natl. Acad. Sci. U.S.A.*, **89**, 3884–3888.
45. Iacomino,G., Picariello,G. and D'Agostino,L. (2012) DNA and nuclear aggregates of polyamines. *Biochim. Biophys. Acta*, **1823**, 1745–1755.
46. Pollard,K.J., Samuels,M.L., Crowley,K.A., Hansen,J.C. and Peterson,C.L. (1999) Functional interaction between GCN5 and polyamines: a new role for core histone acetylation. *EMBO J.*, **18**, 5622–5633.
47. Arora,V.K., Schenkein,E., Murali,R., Subudhi,S.K., Wongvipat,J., Balbas,M.D., Shah,N., Cai,L., Efstathiou,E., Logothetis,C. *et al.* (2013) Glucocorticoid receptor confers resistance to antiandrogens by bypassing androgen receptor blockade. *Cell*, **155**, 1309–1322.
48. Amin,S., Donaldson,I.J., Zannino,D.A., Hensman,J., Rattray,M., Losa,M., Spitz,F., Ladam,F., Sagerstrom,C. and Bobola,N. (2015) Hoxa2 selectively enhances Meis binding to change a branchial arch ground state. *Dev. Cell*, **32**, 265–277.